W.KAUSEL[1)], J.O.NYLANDER[2)], G.NANZ[3)], S.SELBERHERR[3)], H.POETZL[1)]

1) Institut für Allgemeine Elektrotechnik und Elektronik
Dept. for Physical Electronics
Technical University of Vienna
Gußhausstraße 27-29, A-1040 Vienna, AUSTRIA
and Ludwig Boltzmann-Institut für Festkörperphysik

2) Electronics Group, Dept. of Technology
Uppsala University
Box 534, S—751 21 Uppsala, SWEDEN

3) Institut for Microelectronics
Technical University of Vienna
Gußhausstraße 27-29, A-1040 Vienna, AUSTRIA

BAMBI — A Transient 2D-MESFET Model with General Boundary Conditions Including Schottky and Current Controled Contacts

Abstract — Boundary conditions using a current dependent carrier recombination velocity distribution are developed for modeling Schottky contacts by computer-aided physical simulation. In addition a boundary condition in the form of an arbitrary linear combination of voltage and current at the contact is presented. Thus, MESFET-devices with simple circuits connected to device terminals can be simulated by solving additional equations. As an example the switching behavior of a MESFET with drain resistor is investigated.

Introduction

MESFETs are a potential alternative to MOSFETs. MESFETs offer advantages in simplicity of fabrication compared to MOSFETs, because only low temperature processes are required for fabrication. Without any radiation sensitive oxide under the gate MESFETs have been reported to stand up to 100MRad [1] compared to a value of few hundred kRad for MOSFETS. In the MOS case hot carriers may be injected into the oxide. This fixed charge causes degradation of the characteristics. The effective mobility in the channel also tends to be higher in the MES case. The current flows further inside the silicon causing less interaction between carriers and the interface states. MESFETs therefore show little noise similar to JFETs. Due to these advantages concepts for complementary Silicon MESFETs have been investigated as alternative to the traditional CMOS technology [2].

Such investigations urgently ask for the help of device simulation tools with adequate models for Ohmic and Schottky contacts. This paper presents the implementation of boundary conditions for metal-semiconductor contacts and for floating contacts in

the two-dimensional transient device simulator BAMBI [3,4]. The program simulates devices with both geometry and doping profile being arbitrary. According to the drift diffusion theory [5] it solves the three basic semicondutor equations (1–3) together with the two current equations (4,5) using the method of finite–boxes [6].

$$\Delta\psi = -\frac{q}{\varepsilon}(p - n + N_D - N_A) \tag{1}$$

$$\nabla J_n = q(\frac{\partial n}{\partial t} + R_n) \tag{2}$$

$$\nabla J_p = -q(\frac{\partial p}{\partial t} + R_p) \tag{3}$$

$$J_n = qD_n\nabla n - q\mu n\nabla\psi \tag{4}$$

$$J_p = -qD_p\nabla p - q\mu p\nabla\psi \tag{5}$$

The Ohmic Contact

The analysis is based on electrostatic potential, electron and hole concentration (ψ, n, p) presumed as unknowns. Poisson's equation (1) and the two continuity equations (2,3) are numerically solved with a Dirichlet boundary condition for electrons, holes, and electrostatic potential at ohmic contacts. Assuming space charge neutrality directly under the terminal the concentrations are set equal to their thermal equilibrium values. The boundary condition for the electrostatic potential reads

$$V_{term} = \psi - \psi_{bi} \tag{6}$$

$$\psi_{bi} = \pm\frac{kT}{q}ln\left(\frac{|N_D - N_A|}{n_i}\right) \tag{7}$$

where ψ_{bi} denotes the built–in potential and V_{term} the terminal voltage. Simulating contacts with external circuits, V_{term} becomes floating increasing the number of variables to be calculated by one for each floating contact. The additional equations are given by the new mixed boundary condition (8) defining the dependence between contact voltage V_{term} and contact current I_{term}.

$$\alpha \cdot V_{term} + \beta \cdot \left(I_{term} + C\frac{dV_{term}}{dt}\right) = \gamma \tag{8}$$

This is the most general form of the boundary condition which can be handled by our method. Thus, a variety of possibilities for interpretation in mathematical as well as in electrical terms, is offered. Choosing the dimensions of α, β and γ in the correct way several different definitions of the outer circuit diagram can be given using arbitrarily a serial resistive, or a parallel conductive and serial or parallel capacitive loads.

A current driven circuit shown in Fig. 1 (left side) is described by defining $\alpha = G, \beta = 1, \gamma = I_{appl}$. The equivalent voltage driven circuit diagram of Fig. 1 (center) requires the assumption $\alpha = 1$, $\beta = R$, $\gamma = V_{appl}$.

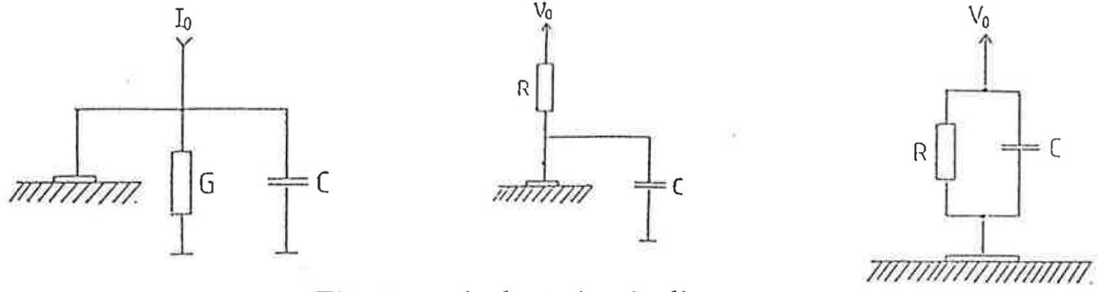

Fig. 1: equivalent circuit diagrams

Interpreting C as a capacity between voltage source and contact (8) has to be slightly modified by the transformation of γ: $\gamma \to \gamma + \beta C \cdot \frac{d(\frac{\gamma}{\alpha})}{dt}$. For a simpler handling by the user (9) has been directly implemented.

$$\alpha \cdot V_{term} + \beta \cdot (I_{term} - C\frac{d\left(\frac{\gamma}{\alpha} - V_{term}\right)}{dt}) = \gamma \tag{9}$$

With the values given above the outer right circuit of Fig. 1 can be simulated.

$$I_{term} = \frac{V_{appl} - V_{term}}{R} + C\frac{d(V_{appl} - V_{term})}{dt} \tag{10}$$

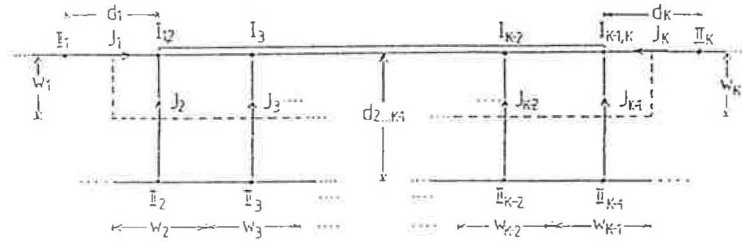

Fig. 2: Discretization of the Boundary Condition

The numerical treatment of mixed boundary conditions (8) or (9) is illustrated by Fig. 2. Both equations include the two variables V_{term} and I_{term} in which V_{term} is the additional unknown and I_{term} has to be expressed by ψ_i, n_i, p_i. The terminal current is given by integrating electron–, hole– and displacement current densities J_n, J_p and J_d over the area of the contact A:

$$I_{term} = \int_A (J_n + J_p + J_d) \cdot dA \tag{10}$$

Using the well known finite difference scheme first suggested by Scharfetter and Gummel [7] the boundary conditions (8) and (9) finally yield the discrete expressions:

$$\alpha \cdot V_{term_T} + \beta \cdot \left(\sum_k (J_{n_k} + J_{p_k} + J_{d_k}) + C\frac{V_{term_T} - V_{term_{T-\Delta T}}}{\Delta T}\right) = \gamma \tag{11}$$

$$\alpha \cdot V_{term_T} + \beta \cdot \left(\sum_k (J_{n_k} + J_{p_k} + J_{d_k}) - \right.$$
$$\left. - C\frac{[(\frac{\gamma}{\alpha})_T - (\frac{\gamma}{\alpha})_{T-\Delta T}] - [V_{term_T} - V_{term_{T-\Delta T}}]}{\Delta T}\right) = \gamma \tag{12}$$

with

$$J_{n_k} = qD_n \frac{w_k}{d_k}[n_{II_k} B(\Delta_k) - n_{I_k} B(-\Delta_k)] \tag{13}$$

$$J_{p_k} = qD_p \frac{w_k}{d_k}[p_{I_k} B(\Delta_k) - p_{II_k} B(-\Delta_k)] \tag{14}$$

$$J_{d_k} = -\frac{w_k}{d_k} \cdot \epsilon \frac{(\psi_{II_k} - \psi_{I_k})_T - (\psi_{II_k} - \psi_{I_k})_{T-\Delta T}}{\Delta T} \tag{15}$$

$$\Delta_k = \frac{\psi_{II_k} - \psi_{I_k}}{V_T}, \quad B(x) = \frac{x}{e^x - 1} \tag{16,17}$$

where I denotes the point at the contact and II the next neighbour (Fig. 2), $J_{n,p,d}$ denote the three current contributions at the midpoints, T the actual time, ΔT the actual time step, d_k the distance between point I and point II and w_k the weighting factor for the integration. D_n and D_p are the coefficients for electron– and hole diffusion, ϵ is the dielectric permittivity, q the electronic charge and V_t the thermal voltage.

Solving the discrete form of the mixed boundary condition (11) and (12), respectively, together with a discrete representation of Poisson's equation and both continuity equations (2,3) yields a numerical solution for electrostatic potential, electron and hole concentration ψ_i, n_i, p_i at each free node in a finite–boxes mesh and the terminal voltage V_{term} for each floating contact. Since (13) and (14) are nonlinear in the unknown variable V_{term} a linearization technique is required. For current or mixed boundary problems the discretized nonlinear equation system is therefore solved simultanously by a coupled Newton's method.

The Schottky Contact

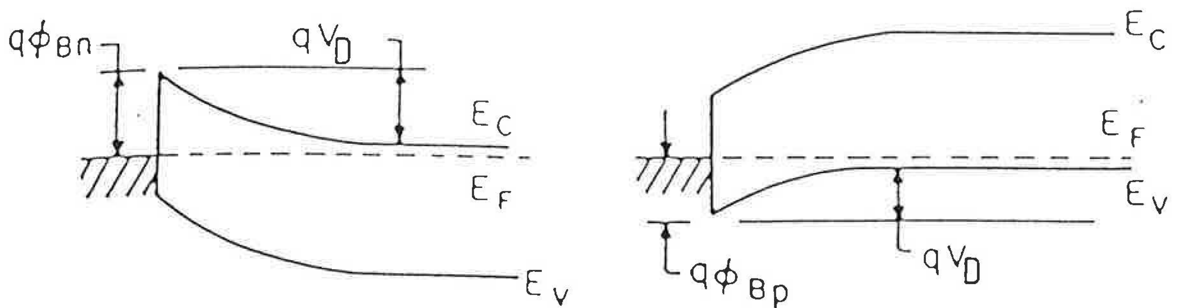

Fig. 3: Diagram of the energy bands at a Schottky contact

When metal is in contact with a semiconductor, potential barriers Φ_{bn} for electrons and Φ_{bp} for holes will be formed at the Metal Semiconductor (MS) interface (Fig. 3). The Fermi levels in the two materials must coincide what causes a depletion layer similar to that of the one–sided abrupt (e.g.,p^+–n) junction. According to the thermionic

emission–diffusion theorie of Crowell and Sze [8] the boundary conditions at the MS– interface read:

$$\psi_i = V_{app} - \psi_s \tag{18}$$

$$J_n = -q \cdot v_n \cdot (n_i - n_o) \tag{19}$$

$$J_p = q \cdot v_p \cdot (p_i - p_o) \tag{20}$$

n_i and p_i are the surface concentrations of electrons and holes, ψ_i the surface potential at the MS–interface, V_{app} the applied voltage and ψ_{bi} the doping dependent built–in voltage (7).

(18) defines the surface potential with the help of the barrier dependent potential value ψ_s (Fig. 3) according to the potential variation within the depletion layer. ψ_s is defined by (21,22)

$$\psi_s = \Phi_{bn} - \Phi_i \tag{21}$$

$$\psi_s = \Phi_i - \Phi_{bp} \tag{22}$$

where Φ_i is the intrinsic energy level.

The boundary conditions (19) and (20) model the carrier flow through the MS–interface with surface recombination terms using effective surface recombination velocities v_n and v_p for electrons and holes, respectively [9].

The quasi–equilibrium concentrations n_0 and p_0 are the surface concentration for zero bias ($V_{appl} = 0$). With (18) the surface potential ψ_i becomes $\psi_i = \psi_s$ yielding

$$n_0 = n_i \cdot \exp(\frac{-\psi_s}{V_T}) \tag{23}$$

$$p_0 = n_i \cdot \exp(\frac{\psi_s}{V_T}) \tag{24}$$

where n_i denotes the intrinsic concentration.

The recombination velocities $v_{n,p}$ at a MS-junction are upper bounded by the saturation velocities of the carriers within the semiconductor and lower bounded by the collection velocity v_c (25). The value of v_c has been derived by Crowell and Sze, assuming a Maxwellian distribution of carrier velocities at the contact.

$$v_c \,|_{(V_{appl} \leq 0)} = \sqrt{\frac{kT}{2m^*\pi}} \cdot f_b f_q \tag{25}$$

$m^*_{n,p}$ is the effective mass for electrons or holes, f_b is the probability of a carrier reaching the metal without being backscattered and f_q is the probability for quantum mechanical reflection of carriers together with tunneling effects.

Defining $v_{n,p}$ equal to a fraction of v_{sat} under forward bias conditions causes unrealistic accumulation of carriers at the MS–interface. Setting $v_{n,p} = v_{sat}$ in order to avoid this accumulation for high forward bias, will result in an unrealistic depletion of carriers at the contact if zero or low bias is applied. As pointed out by Adams [10] one expects a non–Maxwellian distribution of velocities of carriers travelling into the metal.

Our investigations followed the approach by Adams [10] who assumed the carrier velocities to be represented by the positive part of a drifted Maxwellian distribution (26):

$$f(v_x) = K \cdot \exp(\frac{-m^*_{n,p}\gamma_{n,p}(v_x - v_d)^2}{2kT}) \tag{26}$$

Taking the mean value (27)

$$v_{n,p} = \frac{\int_0^\infty v_x f(v_x) dv_x}{\int_0^\infty f(v_x) dv_x} \tag{27}$$

yields the current dependent expression (28)

$$v_{n,p} = v_d + \sqrt{\frac{2kT}{\pi m^*_{n,p}\gamma_{n,p}}} \cdot \frac{\exp(-v_d^2 \cdot \frac{m^*_{n,p}\gamma_{n,p}}{2kT})}{1 + \mathrm{erf}(v_d \cdot \sqrt{\frac{m^*_{n,p}\gamma_{n,p}}{2kT}})} \tag{28}$$

Here $v_d = \frac{J_{n,p}}{q \cdot (n,p)}$ is the drift velocity, $\gamma_{n,p}$ is a compensating factor for the increase of the carrier effective mass caused by band structure changes at the MS interface (Stratton[11]), and K is a normalization constant.

Since the drift velocity is upper bounded by the saturation velocity in the semiconductor, (28) is valid in all practical cases. Comparing the lower bound of (28) for $V_{app} = 0$ with the expression for the collection velocity yields the fitting parameter $\gamma_{n,p} = 4$. Physically this would predict a ratio $\frac{T}{m^*_{n,p}}$ at the MS–interface of 0.25 times the ratio within the semiconductor.

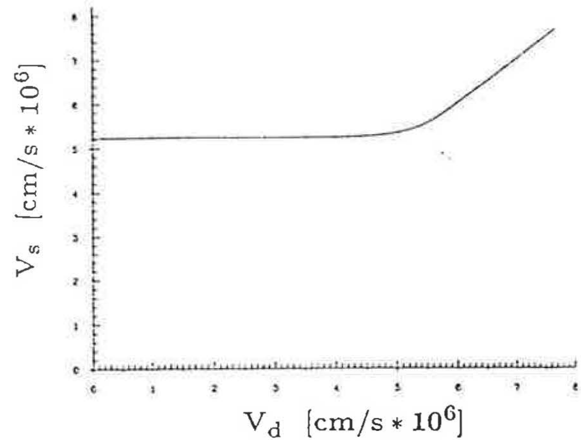

Fig. 4: Recombination velocity vs. drift velocity

Fig. 4 shows the recombination vs. drift velocity. Under reverse bias $v_{n,p}$ are kept constant by neglecting their reduction by f_b and f_q.

Application Example

As a major application the switching behavior of an n–channel Silicon MESFET is presented. Fig. 5 shows the geometry and Fig. 6 the simulated circuit. The gate voltage is switched abruptly from a turn–off voltage $V_G = -2V$ to a turn–on voltage $V_G = 0.2V$. This voltage jump is transmitted to the drain terminal (Fig. 7) resulting in a drain voltage peak of $V_D = 6.78V$ which is at least higher than the supply voltage. The drain current therefore flows out of the device first (Fig. 8). It changes sign after $t = 40ps$ corresponding to the decreasing drain voltage which reaches the value of the supply voltage at the same time. The depleted region under the MES gate (Fig. 9) is reduced from both sides (Fig. 10) but the source current is obviously dominating (Fig. 8,10) due to the limiting drain resistor. During the first $40ps$ the current enters the device through the gate terminal and passes the depletion region as displacement current towards drain and source. After $40ps$ the depletion region is reduced so far (Fig. 11) that an electron convection current starts to flow directly from drain to source. Finally in steady–state condition we observe a broad current pass at that side of the device being opposite to the MES gate (Fig. 12).

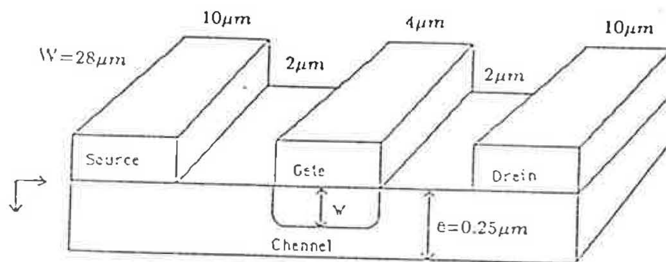

Fig. 5: Geometry of the simulated MESFET

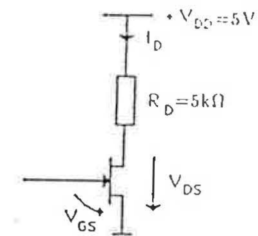

Fig. 6: Simulated circuit

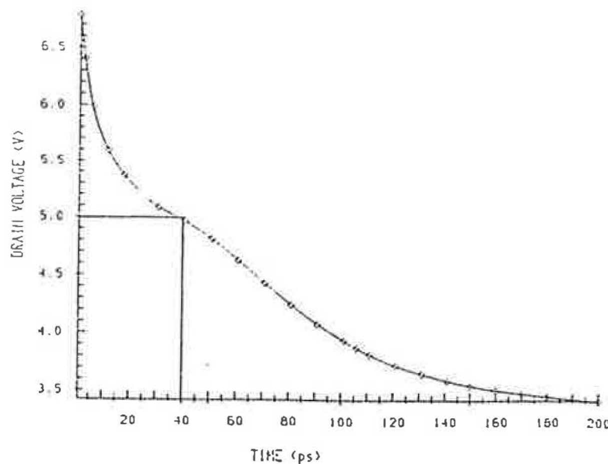

Fig. 7: Drain voltage during turn on

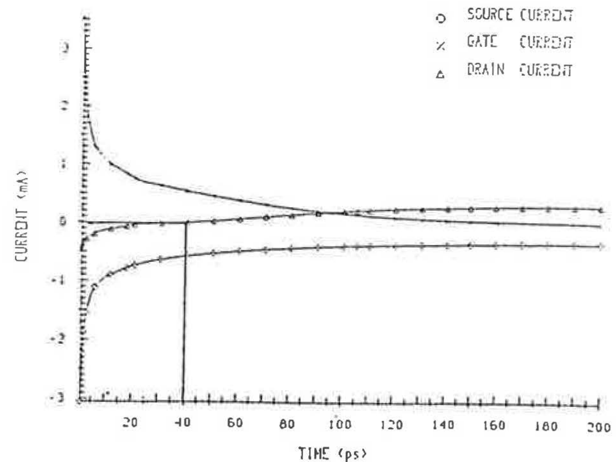

Fig. 8: Contact currents during turn on

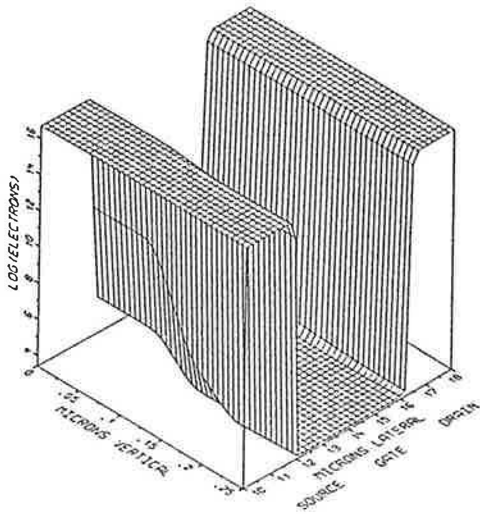

Fig. 9: Electron distribution before turn on

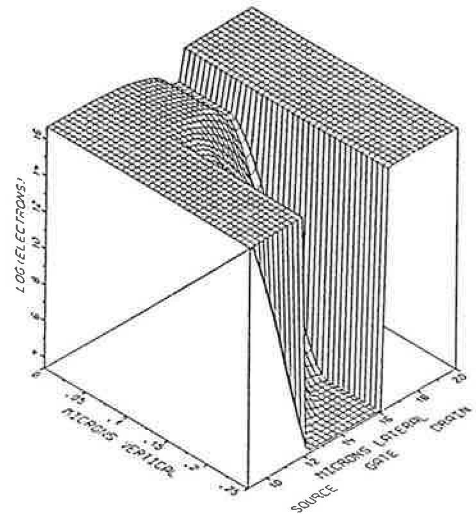

Fig. 11: Electron distribution after 40*ps*

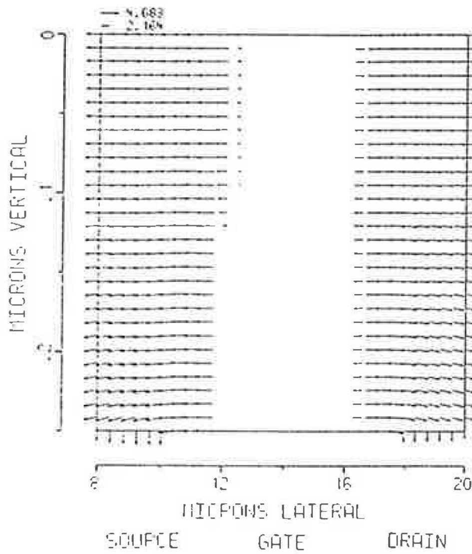

Fig. 10: Electron current density after 1*ps* (logarithmic scale)

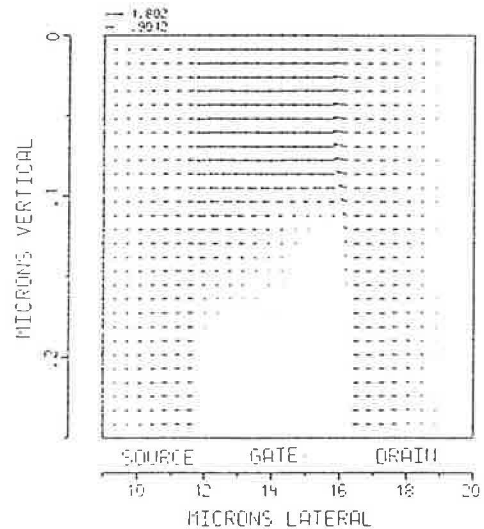

Fig. 12: Steady state electron current density after turn on

Acknowledgement

This work was supported by the SIEMENS AG. Research Laboratories, Munich, Germany and by DIGITAL EQUIPMENT CORP. at Hudson, U.S.A. and by the 'Fond zur Förderung der wissentschaftlichen Forschung', project S43/10. The authors would like to thank the 'Interuniversitäre Rechenzentrum' for supplying the large amount of computer resources.

References

[1] HOUSTON T.W., HITE L.R., DARLEY H.M. et al.
"Radiation Hardness of a Silicon MESFET 4Kx1 sRAM"
in *IEEE Trans. on Nuclear Science*, NS–31, 6, pp.1483, 1984.

[2] BOHLIN K., TOVE P.A.
"Complementary Si MESFET Concept for Logic Circuits."
in *Proc. of the 15th Europ. Solid Dev. Research Conf. ESSDERC 85*, pp. 230-231, Aachen, 1985.

[3] FRANZ A.F., FRANZ G.A., SELBERHERR S.
"BAMBI–A Design Model for Power MOSFET's"
in *Proceedings of the ICCAD Conf.*, pp.179-181, Santa Clara, Ca, 1984.

[4] FRANZ A.F., FRANZ G.A.
"BAMBI–A Design Model for Power MOSFET's"
in *IEEE Trans. on CAD*, Vol.Cad-4, No.3, pp.177-188, Juli 1985.

[5] SZE S.M.: "Basic Equations for Semiconductor–Device Operation"
in *Physics of Semiconductor Devices*, 2nd Ed., J. Wiley & Sons, pp.50, USA, 1981.

[6] FRANZ A.F., FRANZ G.A., SELBERHERR S., RINGHOFER CH., MARKOWICH P.: "Finite Boxes–A Generalization of the Finite–Differences Method Suitable for Semiconductor Device Simulation"
in *IEEE Trans.on Electr.Dev.*, Vol. ED-30, No.9, pp.1070-1082, Sept.1983.

[7] SCHARFETTER D. L., GUMMEL H.K.
"Large–Signal Analysis of a Silicon Read Diode Oscillator"
in *IEEE Trans. on Electr. Dev.*, Vol. ED-16, pp.64-77, 1969.

[8] CROWELL C.R., SZE S.M.
"Current Transport in Metal–Semiconductor Barriers"
in *Solid–State Electronics*, No.9, p.1035, 1965.

[9] CROWELL C.R., BEGUWALA M.,: "Recombination Velocity Effects on Current Diffusion and Imref in Schottky Barriers" in *Solid–State Electronics*, Vol.14, pp.1149-1157, 1971.

[10] ADAMS J., TANG T.: "A Revised Boundary Condition for the Numerical Analysis of Schottky Barrier Diodes" in *IEEE Electr. Dev. Letters*, Vol.EDL-7, No.9, pp.525-527, 1986.

[11] STRATTON R.: "Diffusion of Hot and Cold Electrons in Semicondutor Barriers" in *Physical Review*, Vol.126, pp.2002-2014, 1962.